

Investigation of tunable surface plasmon resonances on spheroid core–shell alloy nanoparticles using DDA method

YUSHAN CHEN, JING LIU*, QIUBO YE, WEI CHEN, CHAOYANG CHEN
School of Information Engineering, Jimei University, Xiamen, Fujian 361021, PR China

In this work, numerical simulations for the absorption and scattering efficiencies of spheroid core–shell nanoparticles (CSNPs) were conducted and studied using the discrete-dipole approximation method. The characteristics of surface plasmon resonances (SPR) depend upon shell thickness, the compositions of the core and shell materials, and the aspect ratio of the constructed CSNPs. We used different core@shell compositions, specifically Au@SiO₂, Ag@SiO₂, Au@TiO₂, Ag@TiO₂, Au@Ag, and Ag@Au, for extinction spectra analysis. We also investigated coupled resonance mode wavelengths by adjusting the composition's layer thickness and aspect ratio. In this study, we show that the extinction efficiency of the Ag@TiO₂ core–shell nanoparticles (CSNPs) was higher than that of the others, and we examined the impact of TiO₂ shell thickness and Ag core radius on SPR peak positions. From the extinction spectra we found that the Ag@TiO₂ nanoparticle had better refractive index sensitivity and figure of merit when the aspect ratio was set to 0.3. All of the experimental results proved that the tunability of these plasmonic resonances was highly dependent on the material used, the layer thickness, and the aspect ratio of the core@shell CSNPs.

(Received September 7, 2018; accepted April 8, 2019)

Keywords: Surface plasmon resonance, Core–shell nanoparticles, Discrete-dipole approximation, Aspect ratio

1. Introduction

Core–shell nanoparticles (CSNPs) are nanostructured materials with interesting characteristics that offer a broad range of applications in optics, biomedicine, environmental science, materials, catalysis, and energy because they have excellent properties such as versatility, tunability, and stability [1-3]. They have attracted tremendous attention for their dramatically tunable optical properties.

Metal nanoparticles (NPs) have special optical properties because they possess more characteristics and functions than the same materials when they are in bulk structures. Smaller particle size gives rise to increased surface-area-to-volume ratios and strong adsorption capacity in the visible region [4]. One of the extremely impressive optical properties of metal NPs is their surface plasmon resonances (SPR). In this situation, optical properties are enhanced and the tunability of these SPR peaks is highly dependent on structural characteristics such as shell thickness, the composition of the core and shell materials, aspect ratio, and the diameter of the spheroidal NPs, as well as their external dielectric environment. However, it is difficult to determine the real influences of these parameters on the optical properties of NPs when we use SPR in various applications, such as optics, biosensors, and medical diagnostics [5].

NPs in complex, multilayer, or core–shell nanostructures have attracted significant interest because they can offer additional opportunities for innovation with

tailored materials in the fields of physics [6], nanomaterials [7], biomedical nanosystems [8], optical chemical sensors [9], magnetic nanocomposites [10], engineering chemistry [11], photocatalysts [12], solar cells [13], and electrical nanosystems [14]. Among these special structures, the core–shell is a particular class of NPs, consisting of a core and one or several shell layers. SPR tunability can be achieved by using different materials to construct the combination of core and shell layers; the diverse applications of CSNPs depend on the core's and shell's properties. Many different categories of CSNPs based on various core and shell materials have been investigated, including CSNPs with metal@metal, metal@dielectric, and dielectric@metal structures [15-17]. The different kinds of CSNPs have attracted plenty of attention, since they have a wide range of applications in different fields, such as photovoltaics and optics, biological labeling, catalysis, photonic crystal creation, optical bioimaging, information storage, and pharmaceuticals [18, 19].

Among the noble metals that exhibit SPR, gold and silver are the most commonly investigated, as they have the most exciting selective absorption in the visible range [20] and their SPR characteristics can easily be adjusted via their size and shape. The synthesis of stable plasmonic NPs is very important, because they have unique surface properties and are suitable for a variety of research fields. In addition, the near-field enhancement of Ag NPs is estimated to be greater than 10 times that of similar Au NPs. Ag NPs are therefore especially attractive

applications in SPR devices. It is well known that metallic Ag is easily oxidized into Ag₂O in air, which has greatly limited its practical application. If a layer of stable oxides is coated on the surface of Ag NPs, the oxidation of Ag NPs can be prevented. Among numerous oxides, TiO₂ has been identified as effective because it has high photocatalytic ability, excellent chemical stability, low toxicity, and low cost [21].

To realize the complementary advantages of Ag and TiO₂ NPs, Pastoriza-Santos et al. first synthesized Ag@TiO₂ CSPs and investigated their properties [22]. They explored a novel method to construct a Ag@TiO₂ CSP nanostructured system, composed of silver cores and a 1–2 nm layer of titanium oxide produced by the simultaneous reduction of silver and condensation of titanium butoxide. A few years later, Sherif et al. tried to explain the contribution that the outer TiO₂ shell made in enhancing the sensitivity of the Ag core. They applied TiO₂, which has a fairly high refractive index of ~ 2.2, as an effective dielectric layer to enhance the sensor sensitivity of the lower Ag layer. They also found that the TiO₂ layer could be a process-compatible protection layer for preventing the Ag substrate from oxidizing [23]. However, the effect of the aspect ratio and size of the CSNPs has not been widely discussed.

To understand the optical behavior of CSNPs, such as their sensitivity and quality factors, the discrete-dipole approximations (DDA) technique can be employed to find the effects of shell thickness and core diameter on the SPR properties of fabricated CSNPs. DDA is one of the most popular numerical analysis tools to calculate the optical properties of designed CSNPs, such as the absorption cross-section, scattering cross-section, and extinction (absorption + scattering) cross-section of metallic NPs and CSNPs with arbitrary shapes, sizes, and structures [24]. In this study, we investigate the relationship between the wavelength and the extinction spectra of coated spheroid CSNPs with different core@shell compositions. To examine and realize the tunability of SPR peaks, we simulate CSNPs of various compositions: Au@SiO₂, Ag@SiO₂, Au@TiO₂, Ag@TiO₂, Au@Ag, and Ag@Au. According to theoretical calculations, we find that the wavelength of the SPR peaks depends on the thickness of the shell layer, the size of the CSNPs, the surrounding environment, and the materials chosen for the core and shell. In addition, we observe the impact of spherical core-shell thickness on the SPR peaks' wavelengths and corresponding spectral widening in distinct regimes of the spectrum. Finally, we explore wavelength variability in the SPR peaks by changing the aspect ratio of the fabricated CSNPs. Through DDA calculations and experimental results, we reach a valuable conclusion.

2. DDA method

The DDA is a convenient method for describing the scattering of light from the surfaces of NPs with arbitrary shapes. In DDA formalism, the object is described as a cubic array lattice of electric dipoles (called N-point

dipoles). In the electric dipoles, the polarizability and position vector of each dipole are specified as α_i and r_i , respectively. The induced dipole polarization P_i in each element is determined from:

$$\mathbf{P}_i = \alpha_i \mathbf{E}_{loc,i}(\mathbf{r}_i), \quad i = 1, 2, \dots, N \quad (1)$$

where the local field $E_{loc,i}(r_i)$ is defined as the sum of the field radiated from all the other N-1 dipoles. For a given special wavelength λ , including the contribution of all the other dipoles, the local field can be written as

$$\mathbf{E}_{loc,i}(\mathbf{r}_i) = \mathbf{E}_0 \exp(i\mathbf{k} \cdot \mathbf{r}_i) - \sum_{\substack{j=1 \\ i \neq j}}^N \mathbf{A}_{ij} \mathbf{P}_j \quad (2)$$

$$i = 1, 2, \dots, N$$

where \mathbf{k} and \mathbf{E}_0 are defined as the wave vector and the amplitude of the incident radiation. The total generated electric field at position i caused by the dipole generated at position j is presented in the second term of equation (2), which can normally be expressed in terms of the dipole-dipole interaction in matrix \mathbf{A} as:

$$\mathbf{A}_{ij} \mathbf{P}_j = \frac{\exp(i\mathbf{k} \cdot \mathbf{r}_{ij})}{r_{ij}^3} \left\{ \begin{array}{l} \mathbf{k}^2 \mathbf{r}_{ij} \times (\mathbf{r}_{ij} \times \mathbf{P}_j) + \\ \left[\frac{1 - i\mathbf{k} r_{ij}}{r_{ij}^2} \times [\mathbf{r}_{ij}^2 \mathbf{P}_j - 3\mathbf{r}_{ij} (\mathbf{r}_{ij} \cdot \mathbf{P}_j)] \right] \end{array} \right\} (j \neq i) \quad (3)$$

when equations (2) and (3) are substituted into (1), the system equation (4) can be generated:

$$\mathbf{A}' \cdot \vec{\mathbf{P}} = \vec{\mathbf{E}} \quad (4)$$

where the off-diagonal elements of the matrix, \mathbf{A}'_{ij} are the same as \mathbf{A}_{ij} for a system with total dipoles, N , whereas,

$\vec{\mathbf{E}}$ and $\vec{\mathbf{P}}$ are 3N-dimensional vectors, and \mathbf{A}' is a 3N×3N matrix. If we solve this set of 3N complex using linear equations, the polarizations $\vec{\mathbf{P}}$ can be determined. We can then calculate the cross-section of the extinction factor as follows:

$$C_{ext} = \frac{4\pi\mathbf{k}}{|\mathbf{E}_0|^2} \sum_{i=1}^N \text{Im}(\mathbf{E}_{loc,i}^* \cdot \mathbf{P}_i). \quad (5)$$

3. Results and discussion

Fig. 1 shows a schematic diagram of the proposed model with different scales in nanometers. The core-shell

structured composite NPs can be viewed as having two parts. One is a nucleus wrapped in the interior of the NPs, and the other is a shell that surrounds the nuclear NPs. R_1 represents the core radius of the core–shell structure, and R_2 represents the radius of the whole core–shell structure, while h is the shell thickness. To explore the SPR characteristics, we used Ag and Au as the core layer of the nanospheroid since they have good extinction properties.

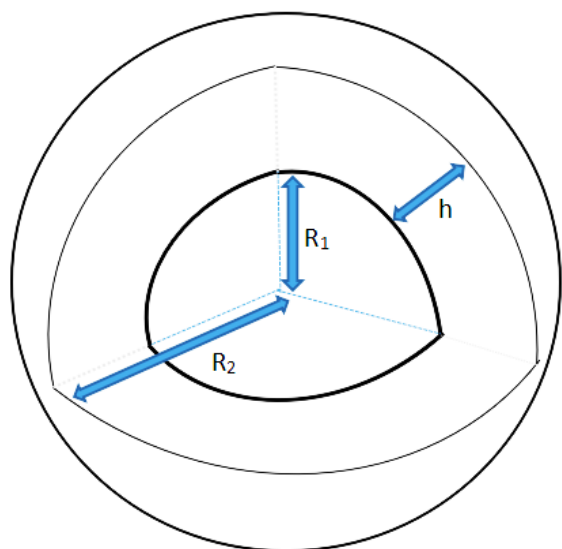


Fig. 1. Schematic diagram of a core–shell structure

In this paper, we investigate three different combinations to achieve spherical CSNPs. The first uses a noble metal (Ag and Au) as the core, and the shell layer is coated with a dielectric material of SiO_2 . The second uses a noble metal (Ag and Au) as the core, and the shell layer is coated with a dielectric material of TiO_2 . The last combination is metal@metal with the structures of Ag@Au and Au@Ag. We demonstrate that by altering the effective radii of the NPs and the thickness of the shell layer, we achieve wide tunability in the wavelengths of the SPR peaks. Using the DDA method, the extinction patterns of these various CSNPs with their different combinations are compared with single noble metal nanospheres (Ag and Au), and the results are shown in Fig. 2.

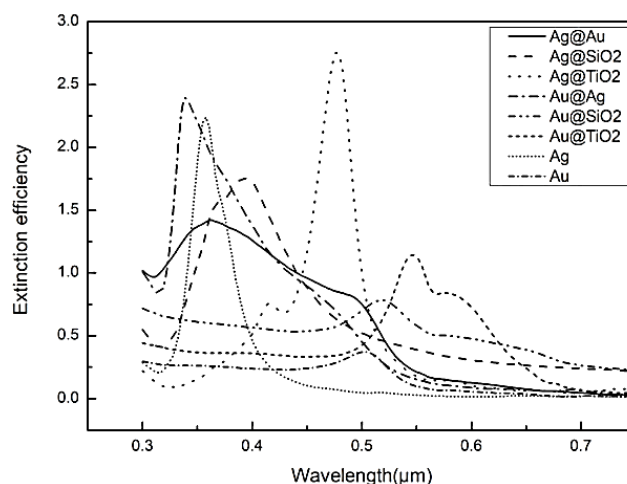


Fig. 2. Comparison of simulation results for various core–shell structures

Extinction efficiency is a parameter used in physics to describe the absorption and scattering of electromagnetic radiation. Any changes in the parameters of metal nanoparticles or nanoparticle arrays could lead to the optical drift in extinction spectrum and thus influence the optical applications in practice. As Fig. 2 shows, the wavelengths of the SPR peaks generated by the CSNPs can be tuned for the spectrum from the visible to the near-infrared region by manipulating the core and shell composition. Compared with uncoated nanospheres, the CSNPs provide an extra degree of freedom in the SPR peaks, meaning that the SPR peaks of the electromagnetic spectra can be tuned and shifted to the desired range. There are many advantages to coating a shell layer on the surfaces of uncoated NPs to form CSNPs structures—stability, surface modification, reduction in consumption of precious materials, and reduction in reactivity. The results shown in the extinction spectra suggest that the Ag@ TiO_2 CSNP structure has the highest sensitivity with different materials. Because the Ag@ TiO_2 CSNPs exhibited the optimum SPR characteristics, we chose them for our follow-up study.

Next, we studied the relationships between the wavelength of an SPR peak and the core radius as well as the shell thickness, since they are important parameters used to tune SPR wavelengths from the ultraviolet to the infrared domain. Fig. 3 shows extinction efficiency versus wavelength for a fixed core ($R_1 = 25$ nm) and various shell thicknesses from 1 to 5 nm, while the corresponding total thickness R_2 was changed from 26 to 30 nm.

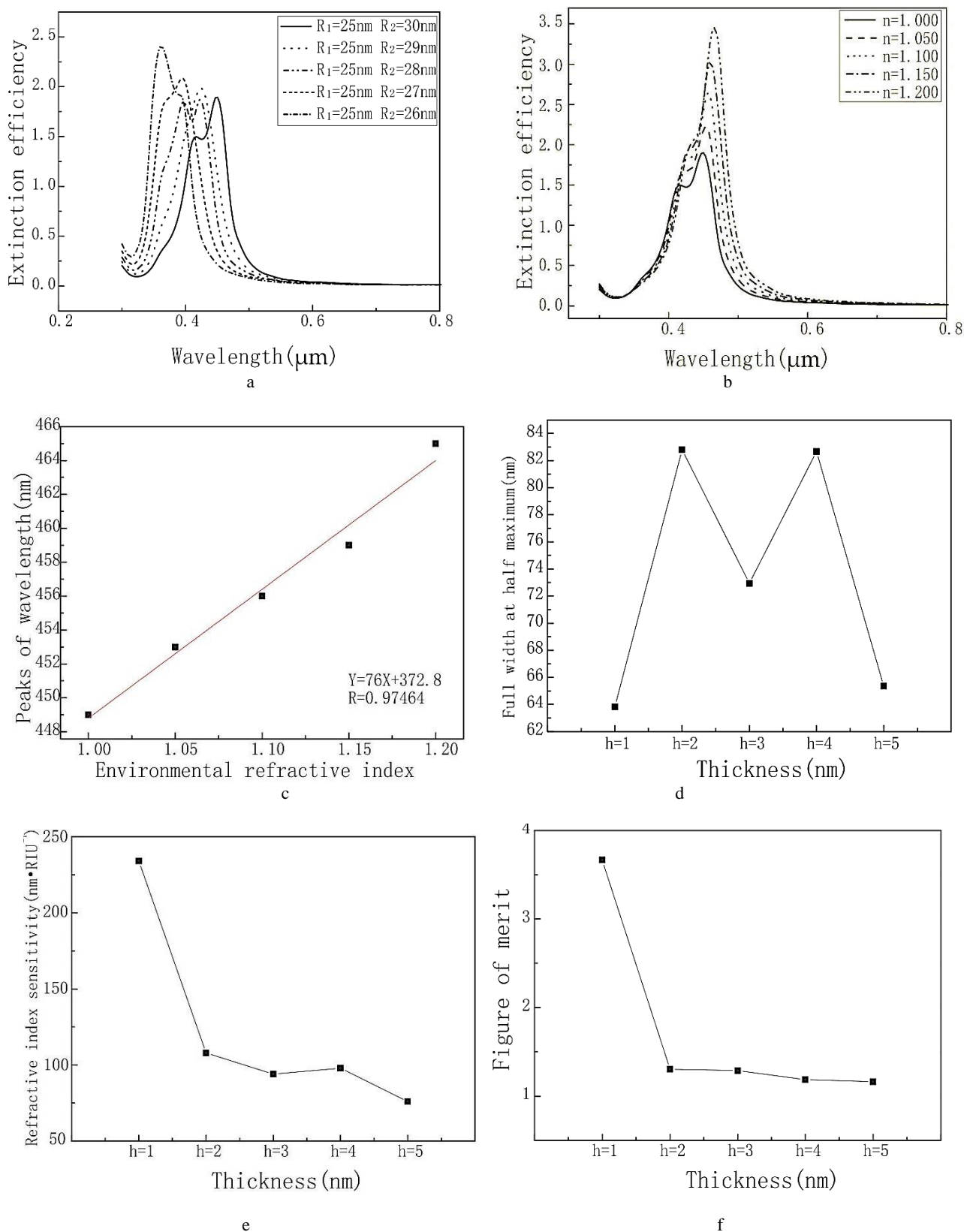


Fig. 3. Calculated results for Ag@TiO₂ core-shell structures: (a) extinction spectra for a fixed core ($R_1 = 25$ nm) with different shell thickness; (b) extinction spectra for a 25 nm Ag layer and 5 nm TiO₂ layer in different media; (c) refractive index sensitivity curve for a 25 nm Ag layer and 5 nm TiO₂ layer; (d) full width at half maximum as a function of shell thickness with a fixed core ($R_1 = 25$ nm); (e) refractive index sensitivity distributions for a fixed core ($R_1 = 25$ nm) with different shell thickness; (f) figure of merit for a fixed core with different shell thicknesses

Fig. 3(a) clearly shows that as the shell layer thickness (h) increased from 1 to 5 nm, the wavelength of the SPR peak shifted from 361 to 448 nm. This result suggests that as the shell layer thickness increases, the extinction spectrum exhibits the red-shift phenomenon, and the extinction peak is gradually reduced. The refractive index sensitivity (RIS) can be defined as $m = \Delta\lambda / \Delta n$ [25], where $\Delta\lambda$ and Δn are the variation in the wavelength of the SPR peak and the variation in the refractive index, respectively. For CSNPs with a diameter of 25 nm for the Ag core and a thickness of 5 nm for the TiO_2 layer, the wavelength of the SPR peak experienced a red shift when the refractive index n increased, as shown in Fig. 3(b). When the refractive index increased from 1.0 to 1.05, the peak wavelength shifted from 449 to 453 nm, exhibiting an RIS of 76 nm/RIU (refractive index unit), as indicated in Fig. 3(c). Fig. 3(e) shows the RIS values of CSNPs with TiO_2 shell layers of different thicknesses.

Based on the calculated results, we prove that the thickness of the TiO_2 layer has a large effect on the RIS value of the Ag@TiO_2 CSNPs. When the thickness increased from 1 to 5 nm, the RIS value critically decreased. These results show that the RIS value of the Ag@TiO_2 CSNPs stays more stable and has a higher value when the thickness of the TiO_2 shell layer is 1 nm. The figure of merit (FOM) value for a metal nanostructure is defined as $p = S/W$ [26], where S and W denote the RIS value and FWHM (full width at half maximum) value, respectively. Using the results in Figs. 3(e) and 3(d), we calculated the FOM values and present the results in Fig. 3(f), which shows that the FOM value decreased as the TiO_2 layer thickness increased from 1 to 5 nm. The maximum FOM value was obtained when the thickness of the TiO_2 layer was set at 1 nm.

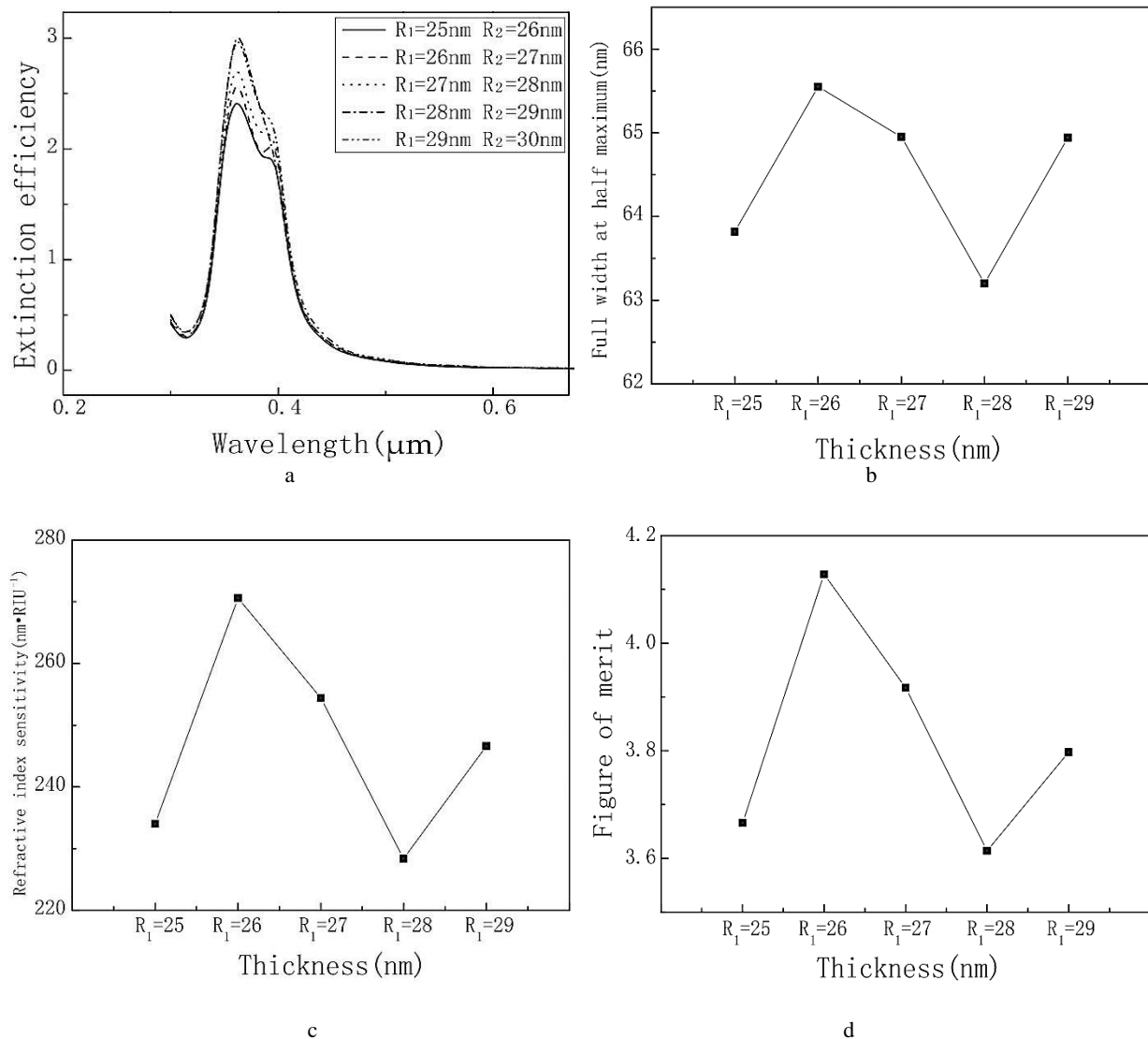


Fig. 4. Calculated results for Ag@TiO_2 core-shell structures with fixed shell thickness ($h = 1$ nm) and different core radii (25–29 nm): (a) extinction spectra; (b) full width at half maximum; (c) refractive index sensitivity distributions; (d) figure of merit

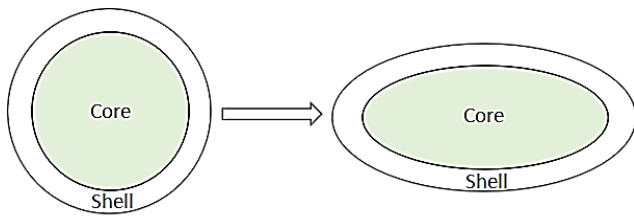


Fig. 5. Changing the aspect ratio of the core-shell structure

We conducted further analysis using a fixed shell thickness (1 nm) and varying the core radius from 25 to 29 nm, to study the effect of core size on the SPR characteristics of Ag@TiO₂ core-shell structures. To observe the extinction properties of the nucleus as its radius increased, we used the DDA algorithm to calculate the results of the extinction spectra; these are shown in Fig. 4(a). Figs. 4(c) and 4(d) represent the RIS and FOM of the Ag@TiO₂ CSNPs with an Ag layer of different thicknesses and a shell thickness (h) of 1 nm. Based on the simulation results, we observe that the RIS and FOM of the Ag@TiO₂ CSNPs are more stable and have optimum performance and higher values when the Ag layer thickness is 26 nm.

It has been reported that SPR peaks in the extinction spectra of CSNPs can also be tuned from the visible light region to the near-infrared region by manipulating their aspect ratio—that is, by changing the aspect ratio of the entire core-shell structure, as shown in Fig. 5. To explore the different aspect ratios in terms of extinction performance, we used an aspect ratio ranging from 0.2 to 1. Based on the DDA method, the resulting extinction spectra are shown in Fig. 6.

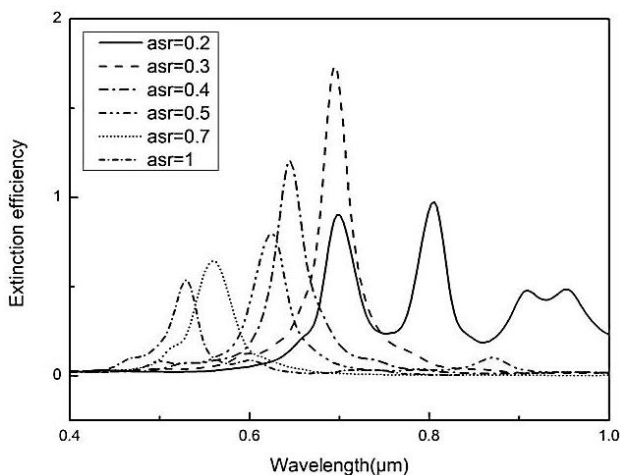


Fig. 6. Extinction spectra for different aspect ratios of the core-shell structure

Fig. 6 shows that the ratio of the minor axis to the major axis (the aspect ratio) played a very important role in optimizing the SPR peak as the ellipsoidal structure was constructed. We compared the extinction spectra of Ag@TiO₂ CSNPs with six different aspect ratios, ranging from 0.2 to 1. The thickness of the TiO₂ shell layer was set at 1 nm while the Ag core radius was set at 26 nm.

In Fig. 6, as the aspect ratio increased from 0.2 to 1, the extinction efficiency increased and simultaneously the resonance frequency shifted to a lower value, showing a blue shift. Consequently, a spectrum with double resonance peaks was revealed, the first peak centered around 702 nm and the second around 810 nm for an aspect ratio of 0.2. We believe that the appearance of these two plasmonic peaks was caused by structural anisotropic effects. When we further increased the aspect ratio, the amplitude of the SPR peak first increased, reaching a maximum aspect ratio of 0.3, and then decreased as the aspect ratio was further increased. In summary, the fluctuations in the surface plasmon resonances with changes in the aspect ratios are caused by the size effect and the aspect ratio of shell layer to core.

4. Conclusion

In this paper, the DDA algorithm was used to simulate the extinction properties of composite nanoparticles with a core-shell structure and proved to be of great significance for the production and preparation of controlled core-shell composite nanoparticles with extinction peaks. Based on the DDA method, we found that the extinction efficiency for Ag@TiO₂ was higher than for other CNNPs (Au@SiO₂, Ag@SiO₂, Ag@TiO₂, Au@Ag, and Ag@Au). The amplitude of the extinction spectrum decreased with increased shell thickness, and the wavelength of the extinction peak increased with increased core layer thickness. In addition, these simulation results showed that the aspect ratio played an important role in modulating the centered wavelength of surface plasmon resonance in the case of a spheroidal nanostructure. The extinction efficiency increased as the aspect ratio decreased, and the extinction peaks underwent a red-shift effect. When we set the aspect ratio to 0.3, we obtained an optimal extinction result. All of these experiments prove that the tunability of these plasmonic resonances is highly dependent on the core@shell material, thickness of shell and surrounding environment while non-coated metal nano-spheres do not show appropriate SPR tunability. The core-shell CNNPs with nanospheroid geometry we proposed in this paper are indeed a viable path for broadband tailoring of surface plasmon resonance, and we expect this to be an effective model forming a hybrid nanoparticle array for high-sensitivity SPR biosensor fabrication.

Acknowledgments

This work was supported by the National Natural Science Foundation of China under Grant Nos. 11505079 and 61505068 and the Education and Scientific Research Project of the Fujian Provincial Education Department under Grant No. FBJG20170137.

Conflicts of Interest

The authors declare that there are no conflicts of interest regarding the publication of this paper.

References

- [1] B. K. Ghosh, N. N. Ghosh, *Journal of Nanoscience and Nanotechnology* **18**, 3735 (2018).
- [2] M. Dabrowski, P. Lach, M. Cieplak, W. Kutner, *Bioelectron* **102**, 17 (2018).
- [3] S. C. Hsu, Y. C. Chuang, B. T. Sneed, D. A. Cullen, T. W. Chiu, C. H. Kuo, *Nano Letters* **16**, 5514 (2016).
- [4] J. Boken, P. Khurana, S. Thatai, D. Kumar, S. Prasad, *Applied Spectroscopy Reviews* **52**, 774 (2017).
- [5] P. Melinon, S. Begin-Colin, J. L. Duvail, F. Gauffre, N. H. Boime, G. Ledoux et al., *Physics Reports-Review Section of Physics Letters* **543**, 163 (2014).
- [6] S. D'Addato, M. C. Spadaro, *Phys. Scr.* **93**, 033001 (2018).
- [7] F. W. Kang, J. J. He, T. Y. Sun, Z. Y. Bao, F. Wang, D. Y. Lei, *Adv. Funct. Mater.* **27**, 1701842 (2017).
- [8] D. Steer, M. Kang, C. Leal, *Nanotechnology* **28**, 142001 (2017).
- [9] S. A. Shahamirifard, M. Ghaedi, M. Montazerzohori, *Applied Organometallic Chemistry* **32**, e4143 (2018).
- [10] N. Shah, F. Claessyns, S. Rimmer, M. B. Arain, T. Rehan, A. Wazwaz et al., *Recent Pat. Nanotechnology* **10**, 202 (2016).
- [11] I. Khalil, S. Rahmati, N. M. Julkapli, W. A. Yehye, *J. Ind. Eng. Chem.* **59**, 425 (2018).
- [12] S. Q. Liu, N. Zhang, Y. J. Xu, *Part. Part. Syst. Charact.* **31**, 540 (2014).
- [13] S. Nayak, C. Mahender, A. Soam, J. Nanda, *Mater. Res. Express* **4**, 105029 (2017).
- [14] J. Q. Wang, S. H. Shin, *J. Nanopart. Res.* **19**, 53 (2017).
- [15] S. Das, A. Paul, A. Chattopadhyay, *Nanoscale* **5**, 9247 (2013).
- [16] S. Das, A. Chattopadhyay, *RSC Adv.* **2**, 10245 (2012).
- [17] P. Li, Y. J. Teng, Y. H. Nie, W. H. Liu, *Food Anal. Meth.* **11**, 69 (2018).
- [18] M. Saliminasab, M. Garaei, R. Moradian, H. Nadgaran, *Plasmonics* **13**, 155 (2018).
- [19] R. Sharma, S. Roopak, N. K. Pathak, A. Ji, R. P. Sharma, *Plasmonics* **12**, 977 (2017).
- [20] Y. Wang, J. Zhai, Y. L. Song, L. He, *Chem. Commun.* **52**, 2390 (2016).
- [21] T. Hirakawa, P. V. Kamat, *Langmuir* **20**, 5645 (2004).
- [22] I. Pastoriza-Santos, D. S. Koktysh, A. A. Mamedov, M. Giersig, N. A. Kotov, L. M. Liz-Marzan, *Langmuir* **16**, 2731 (2000).
- [23] S. H. El-Gohary, M. Choi, Y. L. Kim, K. M. Byun, *Sensors* **16**, 1442 (2016).
- [24] B. T. Draine, P. J. Flatau, *Journal of the Optical Society of America A-Optics Image Science and Vision* **11**, 1491 (1994).
- [25] S. Zhu, C. Du, Y. Fu, *Optical Materials* **31**, 1608 (2009).
- [26] L. J. Sherry, S. H. Chang, G. C. Schatz, R. P. Van Duyne, B. J. Wiley, Y. N. Xia, *Nano Letters* **5**, 2034 (2005).

*Corresponding author: 200761000050@jmu.edu.cn